Mining for protein S-sulfenylation in *Arabidopsis* uncovers redox-sensitive sites

Jingjing Huang[a,b,c,d,e,1,2], Patrick Willems[a,b,f,g,1], Bo Wei[a,b,c,d,e,1], Caiping Tian[h], Renan B. Ferreira[i], Nandita Bodra[a,b,c,d,e], Santiago Agustín Martínez Gache[c,d,e], Khadija Wahni[c,d,e], Keke Liu[h], Didier Vertommen[j], Kris Gevaert[f,g], Kate S. Carroll[i], Marc Van Montagu[a,b,3,4], Jing Yang[h,3,4], Frank Van Breusegem[a,b,3,4], and Joris Messens[c,d,e,3,4]

[a]Department of Plant Biotechnology and Bioinformatics, Ghent University, 9052 Ghent, Belgium; [b]Center for Plant Systems Biology, VIB, 9052 Ghent, Belgium; [c]Center for Structural Biology, VIB, 1050 Brussels, Belgium; [d]Brussels Center for Redox Biology, Vrije Universiteit Brussel, 1050 Brussels, Belgium; [e]Structural Biology Brussels, Vrije Universiteit Brussel, 1050 Brussels, Belgium; [f]Department of Biomolecular Medicine, Ghent University, 9000 Ghent, Belgium; [g]Center for Medical Biotechnology, VIB, 9000 Ghent, Belgium; [h]State Key Laboratory of Proteomics, Beijing Proteome Research Center, National Center for Protein Sciences, Beijing Institute of Lifeomics, 102206 Beijing, China; [i]Department of Chemistry, The Scripps Research Institute, Jupiter, FL 33458; and [j]de Duve Institute, Université Catholique de Louvain, 1200 Brussels, Belgium

Contributed by Marc Van Montagu, August 30, 2019 (sent for review April 22, 2019; reviewed by Bob B. Buchanan, Lars I. Leichert, and Markus Schwarzländer)

Hydrogen peroxide (H_2O_2) is an important messenger molecule for diverse cellular processes. H_2O_2 oxidizes proteinaceous cysteinyl thiols to sulfenic acid, also known as S-sulfenylation, thereby affecting the protein conformation and functionality. Although many proteins have been identified as S-sulfenylation targets in plants, site-specific mapping and quantification remain largely unexplored. By means of a peptide-centric chemoproteomics approach, we mapped 1,537 S-sulfenylated sites on more than 1,000 proteins in *Arabidopsis thaliana* cells. Proteins involved in RNA homeostasis and metabolism were identified as hotspots for S-sulfenylation. Moreover, S-sulfenylation frequently occurred on cysteines located at catalytic sites of enzymes or on cysteines involved in metal binding, hinting at a direct mode of action for redox regulation. Comparison of human and *Arabidopsis* S-sulfenylation datasets provided 155 conserved S-sulfenylated cysteines, including Cys181 of the *Arabidopsis* MITOGEN-ACTIVATED PROTEIN KINASE4 (AtMAPK4) that corresponds to Cys161 in the human MAPK1, which has been identified previously as being S-sulfenylated. We show that, by replacing Cys181 of recombinant AtMAPK4 by a redox-insensitive serine residue, the kinase activity decreased, indicating the importance of this noncatalytic cysteine for the kinase mechanism. Altogether, we quantitatively mapped the S-sulfenylated cysteines in *Arabidopsis* cells under H_2O_2 stress and thereby generated a comprehensive view on the S-sulfenylation landscape that will facilitate downstream plant redox studies.

S-sulfenylation | redox regulation | posttranslational modification | *Arabidopsis* | chemoproteomics

Hydrogen peroxide (H_2O_2) can oxidize specific protein cysteine thiols to sulfenic acid (SOH), a process known as S-sulfenylation. S-sulfenylation functions as an intermediate on the path toward other redox modifications, such as disulfide formation, S-glutathionylation, and overoxidation to sulfinic (SO_2H) and sulfonic (SO_3H) acids (1, 2). A diverse set of reducing enzymes can recycle oxidized cysteines back to their reduced states (3). This reversible oxidation process can govern molecular thiol switches that regulate protein activity, stability, conformational changes, interactions, and cellular location (4–9). Such thiol switch mechanisms can be conserved across species, as demonstrated for cysteine sulfenic acid (Cys-SOH) in human and *Arabidopsis thaliana* glyceraldehyde-3-phosphate dehydrogenases (GAPDHs) (8, 10), methionine sulfoxide reductase B (MsrB) from mouse and *Arabidopsis* (3, 11), and AGC family kinase IRE-1 from *Caenorhabditis elegans* and human (12).

In plants, redox regulation has been documented in diverse signaling processes, such as stress response (13), development (14), cell death (15), and the circadian rhythm (16). Over the last decades, techniques for Cys-SOH detection improved rapidly (2), and 2 identification approaches have been implemented that selectively capture S-sulfenylated proteins in *Arabidopsis* (17–19). One approach uses a plant-optimized genetic YAP1C proteinaceous probe (17, 18) and the other the chemoselective DYn-2 probe (19). Unfortunately, both approaches do not directly identify the modified cysteine residue within the protein. A 1-(pent-4-yn-1-yl)-1H-benzo[c][1,2]thiazin-4(3H)-one 2,2-dioxide (BTD)-based probe that exhibits a superior reactivity with an ~200-fold higher reaction rate than DYn-2 (20), in combination with a quantitative chemoproteomics workflow, had previously been implemented for site-specific S-sulfenylation identification in human cells (21, 22). Here, we successfully applied this approach for global and site-specific profiling of cysteine S-sulfenylation in *Arabidopsis* cells.

Results and Discussion

Chemoproteomics Analysis of S-Sulfenylated Cysteines in *Arabidopsis* Cells. Based on the previously reported protocols (21–23), an adapted chemoproteomics workflow was applied for in situ Cys-SOH

Significance

Cysteine oxidation can induce structural and functional protein alterations in a reversible manner. This process can be regarded as an on-and-off redox switch that regulates cellular signals in plants, but the full repertoire of redox switches remains largely underexplored. The initial oxidation step of a cysteine is known as S-sulfenylation. Thus far, in plants, the current knowledge of S-sulfenylation is mostly limited to the identification of modified proteins. To uncover the S-sulfenylation landscape in *Arabidopsis thaliana* at the cysteine site level, we applied a state-of-the-art chemoproteomics approach in plants and obtained a quantitative S-sulfenylation site inventory that will encourage future structural and functional redox studies.

Author contributions: J.H., M.V.M., J.Y., F.V.B., and J.M. designed research; J.H., B.W., C.T., R.B.F., N.B., S.A.M.G., K.W., D.V., and J.Y. performed research; R.B.F. and K.S.C. contributed new reagents/analytic tools; P.W., K.L., and J.Y. analyzed data; and J.H., P.W., K.G., J.Y., F.V.B., and J.M. wrote the paper.

Reviewers: B.B.B., University of California, Berkeley; L.I.L., Ruhr University Bochum; and M.S., University of Münster.

The authors declare no competing interest.

Data deposition: Mass spectrometry proteomics data are available at the ProteomeXchange Consortium via the PRIDE partner repository under accession numbers PXD013495 (BTD chemoproteomics) and PXD013588 (recombinant *At*MAPK4).

[1]J.H., P.W., and B.W. contributed equally to this work.

[2]Present address: Genetics and Physiology of Microalgae, Université de Liège, 4000 Liège, Belgium.

[3]M.V.M., J.Y., F.V.B., and J.M. contributed equally to this work.

[4]To whom correspondence may be addressed. Email: marc.vanmontagu@ugent.be, yangjing54@hotmail.com, frank.vanbreusegem@psb.vib-ugent.be, or joris.messens@vub.vib.be.

This article contains supporting information online at www.pnas.org/lookup/suppl/doi:10.1073/pnas.1906768116/-/DCSupplemental.

First published October 2, 2019.

detection and quantification in *Arabidopsis* cell cultures in the presence of H_2O_2 (Fig. 1*A*). First, we optimized the Cys-SOH labeling conditions with the BTD probe by varying the H_2O_2 concentrations. Whereas the protein S-sulfenylation levels, reflected by the biotinylation signals on Western blots, increased with the addition of 100 μM to 400 μM BTD, it decreased for H_2O_2 concentrations higher than 100 μM. This decrease in S-sulfenylation levels with increasing H_2O_2 concentrations suggests overoxidation of SOH to $SO_{2/3}H$ (*SI Appendix*, Fig. S1). To capture and identify BTD-labeled peptides, samples were processed by a well-established chemoproteomics workflow (21) (Fig. 1*A*). Specifically, *Arabidopsis* cell cultures were incubated with 400 μM BTD and treated with or without (control) 100 μM H_2O_2 for 25 min. After protein extraction and tryptic digestion, BTD-modified peptides from H_2O_2-treated and control cells were conjugated with light and heavy azido-biotin reagents with an ultraviolet (UV)-cleavable linker, respectively, through a copper-catalyzed alkyne azide cycloaddition reaction (also known as click chemistry) and mixed together in a 1:1 ratio. After enrichment on streptavidin beads and photorelease at 365 nm, the resulting peptides were analyzed by liquid chromatography tandem mass spectrometry (LC-MS/MS) (Fig. 1*A*).

In total, we detected 6,399 peptide-spectrum matches, corresponding to probe-modified peptides in 3 biological replicates, resulting in the identification of 1,537 unique Cys-SOH sites on 1,394 proteins (Fig. 1*B* and Dataset S1). By comparison with the DYn-2 carbon nucleophile and the YAP1C genetic probes, in this study, we mapped 315 Cys-SOH sites of approximately half of the previously identified S-sulfenylation proteins (48.5%, 200 out of 412 proteins) (Fig. 1*B* and Dataset S1). More importantly, an additional 1,222 Cys-SOHs mapped to 1,194 proteins that had not been identified previously (17–19). Taken together, this study represents a detailed compendium of protein S-sulfenylation sites in oxidation-challenged plant cells.

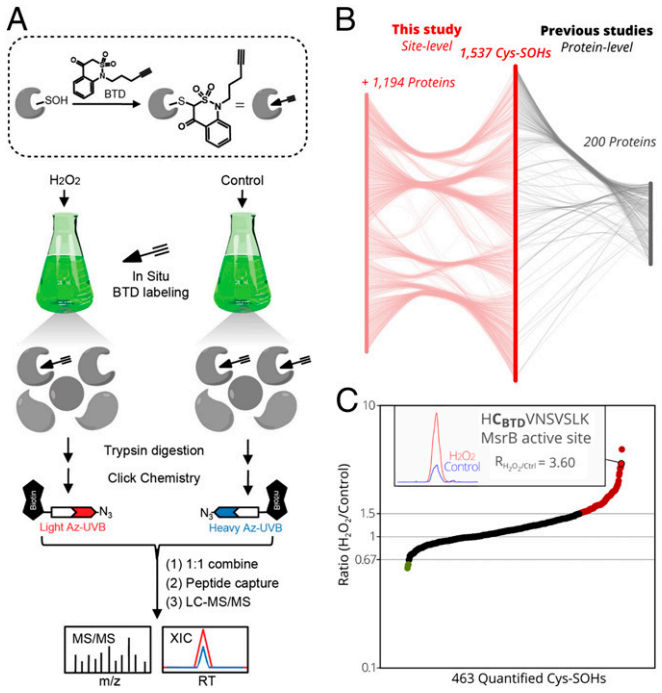

Fig. 1. Quantitative Cys-SOH identification in *Arabidopsis*. (*A*) Workflow for in vivo S-sulfenylation labeling and analysis in *Arabidopsis* cell cultures. The BTD-based probe was sketched as an arrow (chemical warhead) followed by 3 lines indicating the alkyne handle. (*B*) Mapping of the 1,537 identified Cys-SOHs sites on 1,394 (Araport11) proteins, of which 200 proteins were identified to be S-sulfenylated previously (17–19) (*Right*) and 1,194 were discovered as protein targets (*Left*) (Dataset S1). (*C*) Ratios ($R_{H2O2/Control}$, *y* axis) plotted for 463 Cys-SOH sites quantified in at least 2 out of 3 replicates (*x* axis). Ratios of at least 1.5-fold increases (red, 92 Cys-SOHs) or decreases (green, 3 Cys-SOHs) are shown. (*Inset*) For the catalytic Cys of MsrB3/7/8/9 (encircled in bold), the extracted-ion chromatogram is displayed (H_2O_2/light in red, and control/heavy in blue).

Comparison of precursor intensities of light (H_2O_2-treated) and heavy (control) BTD-modified peptide pairs enabled the quantification of 72.4% (1,105) of S-sulfenylation events under H_2O_2 stress, among which 463 sites (~42%) could be quantified in at least 2 out of 3 biological replicates, with median and average relative SD of 6.61% and 8.95%, respectively (*SI Appendix*, Fig. S2). Not unexpectedly, S-sulfenylation levels of ~20% (92/463) of these cysteines increased in *Arabidopsis* cells upon H_2O_2 treatment [H_2O_2 to control ratios, $R_{H2O2/Ctrl} \geq 1.5$, representing a threshold value commonly used in redox proteomics (22, 24, 25) as an indication of significant difference], whereas a majority (79.5%) of Cys-SOHs remained unchanged (Fig. 1*C* and Dataset S1). For instance, the BTD-modified peptide "HC_{BTD}VNSVSLK," which entails the active sites (Fig. 1*C*) of the MsrB3, Msr7, Msr8, and Msr9, shows an elevated intensity upon H_2O_2 treatment ($R_{H2O2/Ctrl} = 3.60$; *SI Appendix*, Fig. S3). It is well known that the formation of a Cys-SOH in the MsrB-active site is an essential step in the catalytic cycle of MsrBs of several species (3, 11, 26). As such, this increased S-sulfenylation on the catalytic cysteine of MsrB results, probably, from an increased MsrB activity due to the applied H_2O_2 stress on the *Arabidopsis* cells. In addition, only 3 Cys-SOHs showed decreased S-sulfenylation levels under H_2O_2 treatment ($R_{H2O2/Ctrl} < 0.67$), as an indication of overoxidation to the sulfinic or sulfonic acids.

Notably, ~58% (642/1105) of the S-sulfenylated sites could be quantified in only one replicate due to the intrinsic limitation of shotgun proteomics in a data-dependent acquisition mode; hence this result should be interpreted with caution. It is also important to note that our chemoproteomics approach is mainly designed for sulfenic acid identification and ratiometric quantification, rather than stoichiometric measurement. As such, a ratiometric increase for a specific site might only correspond to a minor stoichiometric difference. Without doubt, there is a continued need to develop methods that can globally measure site occupancy of this distinct type of cysteine oxidation, although the total cysteine oxidation content can be determined by a well-established chemoproteomics approach designated oxydative isotope-coded affinity tag (27). Furthermore, a more complete picture could be obtained by combining chemoselective probes for oxidized cysteines, as recently done for Cys-SOH (22).

Bioinformatics Analysis on the Target Specificity of S-Sulfenylation. To find targeted processes or protein hotspots sensitive to S-sulfenylation, we first determined the subcellular distribution of the identified S-sulfenylated proteins (Fig. 2*A* and Dataset S1) (28, 29). The best-represented subcellular compartments are cytoplasm (48%), chloroplast (18%), mitochondrion (13%), and nucleus (12%). In comparison to the previous subcellularly oriented cytosolic and plastid YAP1C approaches (17, 18), and the DYn-2 approach (19), the current workflow provides a more diverse spectrum of proteins in terms of subcellular location (*SI Appendix*, Fig. S4).

To dissect the biological processes targeted by S-sulfenylation, we performed gene set enrichment of the 1,394 identified S-sulfenylated proteins for the Kyoto Encyclopedia of Genes and Genomes (KEGG) metabolic pathways and custom protein classes (Dataset S2). It should be noted that, in this over-representation analysis, a certain bias toward abundant protein classes and pathways might arise due to the favorable detection of more-abundant peptide species by MS. Consistent with our previous observations (2, 18, 19), the S-sulfenylated proteins are overrepresented in the essential metabolic pathways (Q value $\leq 1E^{-6}$), such as "carbon metabolism," "glycolysis/gluconeogenesis,"

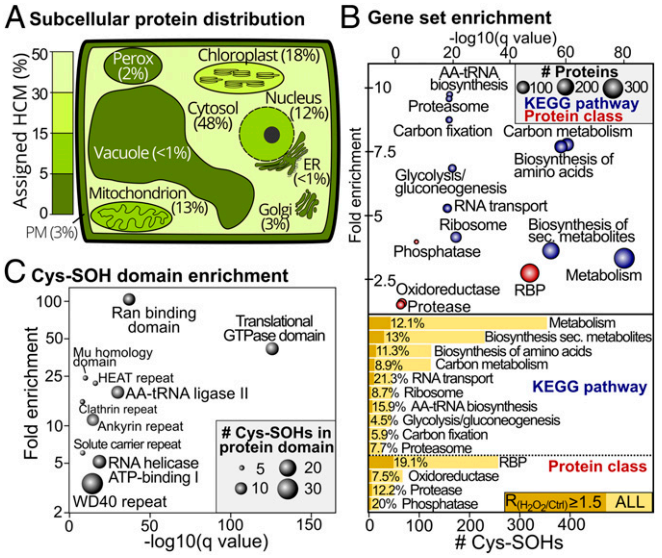

Fig. 2. Subcellular localization distribution and functional enrichment of S-sulfenylation events. (*A*) Subcellular distribution of 809 S-sulfenylated proteins defined as high-confidence markers (HCMs) by the Multiple Marker Abundance Profiling tool (28, 29). Organelles are colored proportionally to the S-sulfenylated HCMs. (*B*) Gene set enrichment of S-sulfenylated proteins for KEGG pathways (blue) and custom protein classes (*SI Appendix, Materials and Methods*) (*Top*). Fold enrichment (*y* axis) is plotted as a function of statistical significance (minus log Q value, *x* axis). Node size corresponds to the number of S-sulfenylated proteins. Bar chart outlining the number of Cys-SOHs for the enriched KEGG pathways and protein classes (*Bottom*). Induced Cys-SOHs ($R_{H2O2/Ctrl} \geq 1.5$) are plotted, and their respective proportion is displayed. (*C*) Cys-SOH domain enrichment (*SI Appendix, Materials and Methods*). Fold enrichment (*y* axis) is plotted as a function of statistical significance (minus log Q value, *x* axis). Node size is scaled to the number of Cys-SOHs. ER, endoplasmic reticulum; PM, plasma membrane.

and "amino acid biosynthesis" (Fig. 2*B* and Dataset S2). RNA-binding proteins (RBPs) (247 out of 1,786 or 13.8%, Q value $\leq 1E^{-46}$) were strongly overrepresented, directly corroborating the observed enrichment of KEGG pathways involved in translation, including "aminoacycl-tRNA (AA-tRNA) biosynthesis," "RNA transport," and "ribosome" (Fig. 2*B* and Dataset S2). Furthermore, several Cys-SOH sites of these RBPs showed an increased S-sulfenylation ($R_{H2O2/Ctrl} \geq 1.5$), with, for instance, 7 out of 44 Cys-SOHs (15.9%) of AA-tRNA synthetases (*SI Appendix*, Table S1). Notably, similar RNA and metabolic processes had been specified as redox-sensitive in human colon cervical alveolar adenocarcinoma cells lines (22, 23), suggesting that these processes are a common S-sulfenylation target across species.

Using the precise knowledge of Cys-SOHs residues, we identified protein domain hotspots sensitive to Cys S-sulfenylation by performing a Cys-SOH protein domain enrichment (Fig. 2*C*) (*SI Appendix, Materials and Methods* and Dataset S2). The high prevalence of RBPs is emphasized further by the strong enrichment of protein domains involved in translation, such as "Translational GTPase," "AA-tRNA ligase II," and "RNA helicase adenosine 5′-triphosphate (ATP)-binding I" domains. In addition, 7 Cys-SOHs are present in the RNA recognition motif (RRM) domain (Dataset S2), including 5 Cys-SOHs that map to poly(A)-binding proteins (PABPs) and contain 4 highly conserved RRM domains in tandem (30). For PABP4, 3 identified Cys-SOHs were located within RRM domains, namely Cys163, Cys266, and Cys357. Given the increase in the Cys163 and Cys357 S-sulfenylation of PABP4 by H_2O_2 stress, Cys-SOH could affect the poly(A)-binding capacity and, hence, translation. Another enriched oxidation-sensitive domain is the Ras-related nuclear protein (Ran)-binding domain (Fig. 2*C*), which is essential for nuclear transport and facilitates nuclear assembly and cell cycle progression (31). Almost all Cys-SOHs in the Ran-binding domain show H_2O_2-increased S-sulfenylation levels (Dataset S1), suggesting a potential redox regulatory role of this Ran-binding domain in the Ran cycle. In addition, the WD40 and Ankyrin repeat domains are also highly enriched (Fig. 2*C*), both mediating protein–protein interactions in diverse signaling processes (32, 33).

S-Sulfenylation at Specific Cysteine Sites Affects Protein Functionality. To estimate the consequences of the identified Cys-SOH sites, we cross-referenced them with known functional sites curated by the UniProt knowledgebase (https://www.uniprot.org/) (34), and obtained 28 functionally annotated Cys-SOHs (*SI Appendix*, Table S2), including 10 sites validated by mutagenesis studies, 3 sites recorded from protein structure analysis, and 15 sites that were inferred in silico based on homology.

From the 10 Cys-SOH sites studied by mutagenesis (*SI Appendix*, Table S2), 6 are located within the protein catalytic site. Redox regulation by S-sulfenylation has already been shown for the catalytic sites of GAPDH C SUBUNIT 1 (GAPC1) (8) and STARCH-EXCESS 4 (SEX4) (4), but potential redox regulation of METACASPASE4 (MC4), NITRILASE 4 (NIT4), UBIQUITIN-PROTEIN LIGASE 1 (UPL1), and LIKE-SEX FOUR 2 (LSF2) remains to be investigated. Besides active sites, Cys-SOHs in Mg-CHELATASE SUBUNIT 1 (CHI1) (35), GLUTAREDOXIN16 (GRXS16) (36), and the peptidyl-prolyl *cis-trans* isomerase CYP20-3 (37) have been implicated in intradisulfide or interdisulfide bonds crucial for protein conformation and enzymatic activity (*SI Appendix*, Table S2). Similarly, S-sulfenylated Cys165 forms a disulfide bridge with Cys150 of TenA_E, based on protein structure information (38) (*SI Appendix*, Fig. S5*A*). In both the ADH1 and ADH2 structures, Cys47 is involved in the coordination of Zn^{2+} in the catalytic site (*SI Appendix*, Fig. S5 *B* and *C*) and was found here as S-sulfenylated. Recently, oxidation of yeast ADH1 Cys47 has been suggested to cause enzymatic inactivation (39), and the redox sensitivity of *Arabidopsis* ADH1 Cys47 has been shown (40). Whereas supply of NAD^+ or NADH cofactors prevented enzymatic inactivation by H_2O_2, Cys47 mutation to Ser abolished the enzymatic activity (40). Hence, the catalytic Zn^{2+} coordination by Cys47 probably acts as a H_2O_2-sensitive switch that can fine-tune the enzymatic activity. Taken together, the identified Cys-SOH in several proteins implies either the formation of a disulfide bond with a neighboring cysteine, loss of metal coordination, or inactivation of a specific activity. However, the detailed functional impact on protein and cellular levels remains largely unspecified and awaits further analysis.

S-Sulfenylation in *Arabidopsis* and Human Protein Orthologs. To compare the *Arabidopsis* study with the reported BTD-labeling profile in human (20), we examined the linear sequence motifs in the environment of the BTD-identified Cys-SOHs by constructing an iceLogo (41), visualizing overrepresented and underrepresented amino acids (Fig. 3*A*). Cysteine residues were clearly underrepresented and mostly predominant at position −3 and +3 relative to the BTD-labeled position. The absence of a cysteine is a stabilizing factor for a SOH, because its close presence mediates disulfide formation (42) (Fig. 3*A*). Remarkably, several basic amino acids surround the BTD cysteine sites. Whereas lysine is prevalent in human, histidine is primarily present in *Arabidopsis* (Fig. 3*A*). Positively charged histidine and lysine residues are the preferred hydrogen-binding partners for cysteines, as they reduce their pK_a and increase their sensitivity to oxidation (43). For instance, the His preceding the active site of SEX4 (*SI Appendix*, Table S2) has been suggested to decrease the pK_a of the Cys198 and to facilitate a thiolate nucleophilic attack (44).

Further, we compared 1,537 Cys-SOH sites from this BTD dataset and those identified by the DYn-2 and BTD probes from human studies (20, 22, 23). After protein sequence alignment of human–*Arabidopsis* orthologs, the relative positions of Cys-SOHs

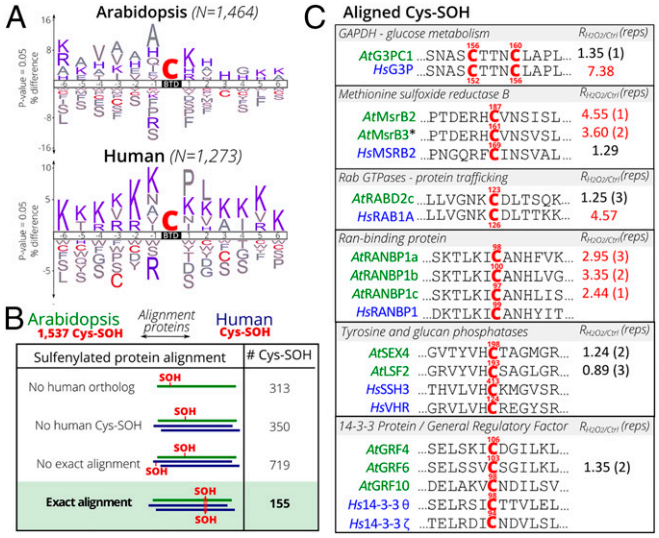

Fig. 3. Evolutionary comparison of *Arabidopsis* and human Cys-SOH sites. (*A*) Overrepresentation motifs of Cys-SOH sequence windows (−6 to +6 residues) of human (20) and *Arabidopsis* BTD-labeled sites constructed by iceLogo (39). Basic residues Lys, Arg, and His are in blue, and Cys is in red. (*B*) Overview of *Arabidopsis* Cys-SOH alignment scenarios and their occurrence. (*C*) Examples of *Arabidopsis* (green)–human (blue) protein sequence alignments with exact alignments of S-sulfenylation events (red, with protein position indicated). Ratios ($R_{H2O2/Ctrl}$) were derived from this study (Dataset S1), with the number of biological replicates indicated between parentheses, and as reported for human RKO cells treated with H_2O_2 (23).

were evaluated, and 4 Cys-SOH alignment categories were distinguished (Fig. 3*B*). In addition to the *Arabidopsis* Cys-SOH sites that lack human protein orthologs (313 Cys-SOHs, 20%) or without S-sulfenylated human orthologs (350 Cys-SOHs, 23%), the majority of the *Arabidopsis* Cys-SOHs does not align exactly with the human Cys-SOH positions (719 Cys-SOHs, 47%). However, 155 *Arabidopsis* Cys-SOH (10%) correspond to those in one or multiple human protein orthologs (Fig. 3*B* and Dataset S1).

These 155 Cys-SOH sites match exactly the human–*Arabidopsis* orthologs, possibly indicating that these sites are conserved oxidation-sensitive sites. Moreover, for some of these proteins, Cys redox regulation has been documented in different species, such as for the catalytic Cys site of GAPDH (8, 10) and MsrB (3, 11) (Fig. 3*C*). Remarkably, in the case of GAPDH, oxidation-sensitive sites were assigned to 2 adjacent cysteines (Cys156 and Cys160) (*SI Appendix*, Fig. S6). Furthermore, the NKCD motif of Ras GTPases has been reported to be redox-sensitive (45, 46), and S-sulfenylation of Cys126 of recombinant human Rab-1A was confirmed with the carbon nucleophilic probe DAz-2 (47), but no information is available yet for the plant orthologs. The conserved Cys-SOHs of the human RAN-BINDING PROTEIN 1 (RANBP1) and its 3 *Arabidopsis* orthologs are located within the Ran-binding domains (Fig. 3*C*). In human, cellular stress and elevated H_2O_2 levels disrupt the Ran system, and this was partly attributed to cysteine oxidation of the nucleotide exchange factor RCC1, although independent mechanisms were suggested (48). Cys-SOH in the active sites of *At*LSF2 and *At*SEX4 (*SI Appendix*, Table S2) align with the nucleophilic Cys of 2 human Protein Tyr Phosphatases (PTPs), VACCINIA H1-RELATED PHOSPHATASE (*Hs*VHR) and SLINGSHOT HOMOLOG3 (*Hs*SSH3) (Fig. 3*C*). Low H_2O_2 concentrations were reported to oxidize and inactivate *Hs*VHR reversibly (49). Another human PTP, *Hs*SSH1, is activated under oxidative stress due to Cys oxidation of its negative interactor *Hs*14-3-3ζ (50). The Cys94 of *Hs*14-3-3ζ was identified as oxidation-sensitive, and its mutation to Ala or Ser causes significant protein destabilization (51). Notably, 3 S-sulfenylated cysteines from the *Arabidopsis* orthologous proteins, general regulatory factors, align with Cys94 of *Hs*14-3-3ζ (Fig. 3*C*). To explain potential functional roles of these cysteines, comparison of Cys-SOH sites between protein orthologs can help prioritizing cysteine functional sites for mutagenesis studies.

Functional Importance of Cys181 in *At*MAPK4. *Arabidopsis* mitogen-activated protein kinases (*At*MAPKs) play important roles in plant signaling (52) and have been shown to be activated by H_2O_2 (53–56), although the precise mechanism remains elusive. Among the 155 Cys-SOH sites that exactly match the human–*Arabidopsis* orthologs (Fig. 3*B* and Dataset S1), a Cys-SOH site occurred in a unique peptide "DLKPSNLLLNANC$_{BTD}$DLK" (*SI Appendix*, Fig. S7) that can be mapped to several *At*MAPKs, including *At*MAPK3, *At*MAPK4, *At*MAPK6, and *At*MAPK11, of which *At*MAPK4 had previously been trapped by the YAP1C probe (18). The identified S-sulfenylated Cys from *At*MAPK4, Cys181, resides in a conserved motif (MAP Kinase signature) that distinguishes MAPKs from other kinases (Fig. 4*A*) (57). Our comparative analysis with the human Cys-SOHs indicated an exact alignment with Cys161 of *Hs*MAPK1 (Fig. 4*A*), also known as EXTRACELLULAR SIGNAL-RELATED KINASE2 (*Hs*ERK2). Besides sequence alignment, superimposing a structural model of *At*MAPK4, based on the structure of *At*MAPK6 (58), with *Hs*MAPK1 (59) revealed an almost identical structural environment of Cys181 in *At*MAPK4 and Cys161 in *Hs*MAPK1 (*SI Appendix*, Fig. S8). For both structures, a conserved proximal His (*At*MAPK4 His145, *Hs*MAPK1 His125) acts as a possible hydrogen bond donor and could thereby decrease the pK_a of the thiol by stabilizing it as a thiolate (43), which increases the oxidation sensitivity of the cysteines (*SI Appendix*, Fig. S8). Notably, Cys161 resides in a conserved docking site that governs the regulatory protein interactions of *Hs*MAPK1 (60–62).

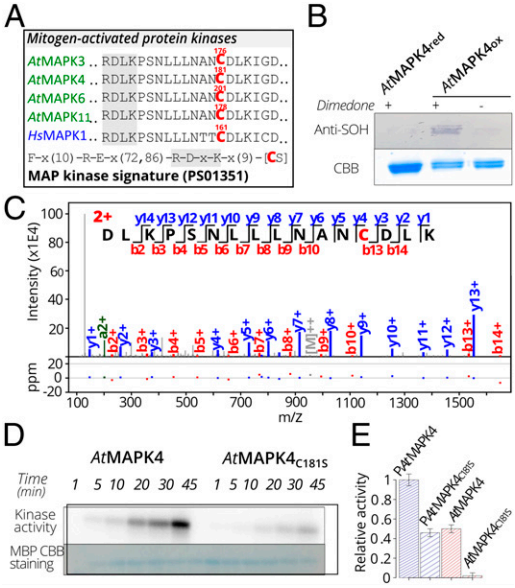

Fig. 4. Sulfenylation of Cys181 of *At*MAPK4 that is crucial for the kinase activity. (*A*) S-sulfenylation of the H_2O_2-sensitive Cys in the MAP kinase signature (PS01351 PROSITE pattern) in *Arabidopsis* (Cys176 in *At*MAPK3; Cys181 in *At*MAPK4; Cys201 in *At*MAPK6; and Cys178 in *At*MAPK11) and human (Cys161 in *Hs*MAPK1). (*B*) Dimedone blot showing *At*MAPK4 S-sulfenylation under 1 mM H_2O_2 for 1 h. (*C*) Annotated spectrum match of 'DLKPSNLLLNANC$_{181}$DLK' with Cys181 modified by dimedone (+138.0 Da). (*D*) Kinase activity of *At*MAPK4 and its C181S variant as measured on phosphorimage displaying myelic basic protein (MBP) phosphorylation with [^{32}P]ATP. (*E*) Kinase activity of autophosphorylated (P_i) and nonautophosphorylated *At*MAPK4 and its C181S variant as measured by quantitative Cerenkov counting after 45 min of incubation with MBP.

In recombinant *Hs*MAPK1, S-sulfenylation was reported to decrease kinase activity toward a substrate protein, Elk1, with Cys161 and/or Cys166 proposed as potential oxidation-sensitive sites that could influence kinase activity given their location within the docking site (63). Noteworthy, the *Hs*MAPK1 Cys166 corresponds to Gly in *Arabidopsis* MAPKs; hence, we decided to investigate the functional effect of *At*MAPK4 Cys181 that corresponds to the *Hs*MAPK1 Cys161. First, we confirmed the S-sulfenylation of H_2O_2-oxidized recombinant *At*MAPK4 with dimedone blots (18) (Fig. 4*B*) and the maintenance of its overall structure upon oxidation with far UV circular dichroism (CD) (*SI Appendix*, Fig. S9). MS/MS analysis showed that Cys181 of the recombinant *At*MAPK4 was consistently detected as oxidation-sensitive (Fig. 4*C*) as other cysteines (Cys6, Cys181, Cys232, and Cys341) (*SI Appendix*, Table S3 and Dataset S3). To study the functional effect of only Cys181, which was identified as redox-sensitive in vivo, we mutated Cys181 into serine (*At*MAPK4$_{C181S}$). Similarly to the oxidized *At*MAPK4, CD spectra indicated a conserved secondary structure composition without drastic structural alterations, due to the Cys181 mutagenesis of *At*MAPK4 (*SI Appendix*, Fig. S10). Next, kinase activities were evaluated by the incorporation of [γ-^{32}P] ATP in the myelin basic protein (Fig. 4 *D* and *E*). In the *At*MAPK4$_{C181S}$ variant, the kinase activity was significantly lower than that of the wild-type *At*MAPK4 (Fig. 4 *D* and *E*), implying that Cys181 affects the *At*MAPK4 kinase activity. As MAPK family proteins can also be phosphorylated on specific Tyr/Thr/Ser residues (64), we identified Tyr203 of recombinant *At*MAPK4 to be prone to autophosphorylation (*SI Appendix*, Table S3 and Dataset S3). Tyr203 belongs to a conserved TEY amino acid activation segment of the TEY subgroup of MAP kinases. Therefore, we made sure that both enzymes were compared in exactly the same experimental setup to allow the control of autophosphorylation (Fig. 4*E*). Control of the autophosphorylation confirmed the decrease of the kinase activity for the *At*MAPK4$_{C181S}$ variant. Taken together, the oxidation-sensitive Cys181 of *At*MAPK4 seems to play an important role in the kinase activity, but how Cys181 regulates the *At*MAPK4 activity is still unclear, especially because Cys181 is located remotely from the active site. To investigate the precise role of Cys181 in the kinase mechanism, experiments with *At*MAPK4 native substrates and its MAP kinase kinase within its in vivo redox environment will be required.

Conclusion

Cysteine oxidation is a sensitive and rapid way to alter protein functions. Here, we provide an extensive inventory of S-sulfenylated cysteine sites in *Arabidopsis*. We found that cysteines located at catalytic and metal-binding sites of proteins involved in RNA and metabolic processes are sensitive to oxidation and might be redox-regulated. Further, the comparative analysis between human and plants provides a catalog of conserved S-sulfenylated cysteines, supportive for their potential redox functionality. To validate the outcome of this analysis, we showed that a conserved oxidation-sensitive cysteine in a MAPK plays a significant role in the kinase mechanism. In summary, by uncovering the cysteine S-sulfenylation landscape in *Arabidopsis*, we reach out to the plant redox signaling community, and we are convinced that this study will give rise to future redox-inspired functional studies.

Materials and Methods

***Arabidopsis* Cell Cultures, BTD Labeling, and Stress Treatment.** *A. thaliana* (L.) Heynh. dark-grown cell suspension (PSB-D) lines were cultivated as described (65). Cell suspension cultures at midlog phase (3 d old, OD_{600} = 0.9) were used for the chemoproteomics workflow. The BTD chemical probe was synthesized as described (20). Midlog phase PSB-D cell cultures were incubated with dimethyl sulfoxide and 100 μM or 400 μM BTD, and treated with 0, 0.1, or 1 mM H_2O_2 (Merck Millipore) for 25 min. BTD was added 5 min before the H_2O_2 treatment.

Protein Extraction. After BTD incubation and stress treatments, cells were harvested by filtration and washed 3 times with culture medium. Proteins were extracted according to adapted protocols (21, 66). Additional information is provided in *SI Appendix, Materials and Methods*.

Western Blot Analysis. Protein pellets were resuspended in PBS buffer containing 0.4% (wt/vol) sodium dodecyl sulfate (SDS). Protein concentrations were determined with the Pierce bicinchoninic acid protein kit (Thermo Fisher Scientific). Dissolved proteins (100 μg) were reconstituted in a click reaction solution containing 0.1 mM azido-biotin, 0.25 mM $CuSO_4$, 0.5 mM 3-(4-((bis((1-tert-butyl-1H-1,2,3-triazol-4-yl)methyl)amino)methyl)-1H-1,2,3-triazol-1-yl) propan-1-ol (BTTP), and 2.5 mM ascorbate. The mixture was rotated in the dark for 1 h at room temperature, and the reaction was stopped by incubation with 1 mM ethylenediaminetetraacetic acid for 5 min at room temperature. The reaction mix was separated by SDS-polyacrylamide gel electrophoresis, blotted, and hybridized with a 1:40,000 dilution of horseradish peroxidase -conjugated streptavidin (HRP-Strep).

BTD-Based Chemoproteomics. Preparation and identification of BTD-modified peptides were adapted from previous protocols (21–23). An Orbitrap Fusion mass spectrometer (Thermo Fisher Scientific) operated with an Easy-nLC1000 system (Thermo Fisher Scientific) was used for LC-MS/MS analyses. Raw MS data were searched with the pFind Studio 3.0 software package. The MS proteomics data have been deposited to the ProteomeXchange Consortium via the PRoteomics IDEntification (PRIDE) partner repository (67) with the dataset identifier PXD013495. Additional information is provided in *SI Appendix, Materials and Methods*.

Bioinformatics. A detailed description of the bioinformatic analyses is provided in *SI Appendix, Materials and Methods*.

***AtMAPK4*-Recombinant Protein Expression and Purification.** The coding sequences of *At*MAPK4 (AT4G01370) and its *At*MAPK4$_{C181S}$ mutant were inserted into the pDEST17 vector (Life Technologies). The recombinant protein with His-tag was expressed in the *Escherichia coli* C41(DE3) strain and purified by Ni^{2+} Sepharose column (GE Healthcare). Additional information is provided in *SI Appendix, Materials and Methods*.

In Vitro Dimedone Detection of S-Sulfenylation. Reduced *At*MAPK4 proteins (20 μM) were incubated with 2 mM dimedone. For *At*MAPK4 oxidation, 1 mM H_2O_2 was incubated at room temperature for 1 h. The in vitro dimedone labeling and detection by Western blot and LC-MS/MS were as described previously, with adaptations (68). For additional information, see *SI Appendix, Materials and Methods*.

ACKNOWLEDGMENTS. We thank Gustavo J. Gutierrez for help with kinase assays. This work was supported by the National Key R&D Program of China (project no. 2016YFA0501303 to J.Y.); the Research Foundation-Flanders–Fonds de la Recherche Scientifique (Excellence of Science project no. 30829584 to D.V., K.S.C., F.V.B., J.M., and Claire Remacle), the Research Foundation-Flanders (grants G0D7914N to F.V.B. and J.M., G003809N to K.G. and F.V.B., G055416N and G06916N to F.V.B., and 1508316N to Dr. Inge Van Molle for the purchase of an anaerobic work station), the China Scholarship Council (CSC no. 201606690036 to B.W.), and the Ghent University Special Research Fund (BOF Grant 01J11311 to F.V.B.). J.H. is indebted to the Research Foundation-Flanders for a postdoctoral fellowship (no. 1227020N).

1. C. E. Paulsen, K. S. Carroll, Cysteine-mediated redox signaling: Chemistry, biology, and tools for discovery. *Chem. Rev.* **113**, 4633–4679 (2013).
2. J. Huang, P. Willems, F. Van Breusegem, J. Messens, Pathways crossing mammalian and plant sulfenomic landscapes. *Free Radic. Biol. Med.* **122**, 193–201 (2018).
3. L. Tarrago *et al.*, Regeneration mechanisms of *Arabidopsis thaliana* methionine sulfoxide reductases B by glutaredoxins and thioredoxins. *J. Biol. Chem.* **284**, 18963–18971 (2009).
4. L. N. Sokolov, J. R. Dominguez-Solis, A.-L. Allary, B. B. Buchanan, S. Luan, A redox-regulated chloroplast protein phosphatase binds to starch diurnally and functions in its accumulation. *Proc. Natl. Acad. Sci. U.S.A.* **103**, 9732–9737 (2006).
5. Y. Tada *et al.*, Plant immunity requires conformational changes [corrected] of NPR1 via S-nitrosylation and thioredoxins. *Science* **321**, 952–956 (2008). Erratum in: *Science* **325**, 1072 (2009).
6. Y. Tian *et al.*, Hydrogen peroxide positively regulates brassinosteroid signaling through oxidation of the BRASSINAZOLE-RESISTANT1 transcription factor. *Nat. Commun.* **9**, 1063 (2018).
7. H.-M. Yuan, W.-C. Liu, Y.-T. Lu, CATALASE2 coordinates SA-mediated repression of both auxin accumulation and JA biosynthesis in plant defenses. *Cell Host Microbe* **21**, 143–155 (2017).

8. M. Bedhomme *et al*., Glutathionylation of cytosolic glyceraldehyde-3-phosphate dehydrogenase from the model plant *Arabidopsis thaliana* is reversed by both glutaredoxins and thioredoxins *in vitro*. *Biochem. J.* **445**, 337–347 (2012).
9. B.-W. Yun *et al*., *S*-nitrosylation of NADPH oxidase regulates cell death in plant immunity. *Nature* **478**, 264–268 (2011).
10. D. Peralta *et al*., A proton relay enhances H_2O_2 sensitivity of GAPDH to facilitate metabolic adaptation. *Nat. Chem. Biol.* **11**, 156–163 (2015).
11. G. Kim, R. L. Levine, A methionine residue promotes hyperoxidation of the catalytic cysteine of mouse methionine sulfoxide reductase A. *Biochemistry* **55**, 3586–3593 (2016).
12. J. M. Hourihan, L. E. Moronetti Mazzeo, L. P. Fernández-Cárdenas, T. K. Blackwell, Cysteine sulfenylation directs IRE-1 to activate the SKN-1/Nrf2 antioxidant response. *Mol. Cell* **63**, 553–566 (2016).
13. F. K. Choudhury, R. M. Rivero, E. Blumwald, R. Mittler, Reactive oxygen species, abiotic stress and stress combination. *Plant J.* **90**, 856–867 (2017).
14. A. Mhamdi, F. Van Breusegem, Reactive oxygen species in plant development. *Development* **145**, dev164376 (2018).
15. F. Van Breusegem, J. F. Dat, Reactive oxygen species in plant cell death. *Plant Physiol.* **141**, 384–390 (2006).
16. C. R. Guadagno, B. E. Ewers, C. Weinig, Circadian rhythms and redox state in plants: Till stress do us part. *Front. Plant Sci.* **9**, 247 (2018).
17. B. De Smet *et al*., *In vivo* detection of protein cysteine sulfenylation in plastids. *Plant J.* **97**, 765–778 (2019).
18. C. Waszczak *et al*., Sulfenome mining in *Arabidopsis thaliana*. *Proc. Natl. Acad. Sci. U.S.A.* **111**, 11545–11550 (2014).
19. S. Akter *et al*., DYn-2 based identification of *Arabidopsis* sulfenomes. *Mol. Cell. Proteomics* **14**, 1183–1200 (2015).
20. V. Gupta, J. Yang, D. C. Liebler, K. S. Carroll, Diverse redoxome reactivity profiles of carbon nucleophiles. *J. Am. Chem. Soc.* **139**, 5588–5595 (2017).
21. L. Fu, K. Liu, R. B. Ferreira, K. S. Carroll, J. Yang, Proteome-wide analysis of cysteine *S*-sulfenylation using a benzothiazine-based probe. *Curr. Protoc. Protein Sci.* **95**, e76 (2019).
22. S. Akter *et al*., Chemical proteomics reveals new targets of cysteine sulfinic acid reductase. *Nat. Chem. Biol.* **14**, 995–1004 (2018).
23. J. Yang, V. Gupta, K. S. Carroll, D. C. Liebler, Site-specific mapping and quantification of protein S-sulphenylation in cells. *Nat. Commun.* **5**, 4776 (2014).
24. X. Deng *et al*., Proteome-wide quantification and characterization of oxidation-sensitive cysteines in pathogenic bacteria. *Cell Host Microbe* **13**, 358–370 (2013).
25. J. Guo *et al*., Proteome-wide light/dark modulation of thiol oxidation in cyanobacteria revealed by quantitative site-specific redox proteomics. *Mol. Cell. Proteomics* **13**, 3270–3285 (2014).
26. B. Ezraty, A. Gennaris, F. Barras, J. F. Collet, Oxidative stress, protein damage and repair in bacteria. *Nat. Rev. Microbiol.* **15**, 385–396 (2017).
27. L. I. Leichert *et al*., Quantifying changes in the thiol redox proteome upon oxidative stress in vivo. *Proc. Natl. Acad. Sci. U.S.A.* **105**, 8197–8202 (2008).
28. C. M. Hooper *et al*., Multiple marker abundance profiling: Combining selected reaction monitoring and data-dependent acquisition for rapid estimation of organelle abundance in subcellular samples. *Plant J.* **92**, 1202–1217 (2017).
29. C. M. Hooper, I. R. Castleden, S. K. Tanz, N. Aryamanesh, A. H. Millar, SUBA4: The interactive data analysis centre for Arabidopsis subcellular protein locations. *Nucleic Acids Res.* **45**, D1064–D1074 (2017).
30. D. A. Belostotsky, Unexpected complexity of poly(A)-binding protein gene families in flowering plants: Three conserved lineages that are at least 200 million years old and possible auto- and cross-regulation. *Genetics* **163**, 311–319 (2003).
31. S.-H. Kim, D. Arnold, A. Lloyd, S. J. Roux, Antisense expression of an Arabidopsis Ran binding protein renders transgenic roots hypersensitive to auxin and alters auxin-induced root growth and development by arresting mitotic progress. *Plant Cell* **13**, 2619–2630 (2001).
32. J. Li, A. Mahajan, M.-D. Tsai, Ankyrin repeat: A unique motif mediating protein–protein interactions. *Biochemistry* **45**, 15168–15178 (2006).
33. C. Xu, J. Min, Structure and function of WD40 domain proteins. *Protein Cell* **2**, 202–214 (2011).
34. UniProt Consortium, UniProt: A worldwide hub of protein knowledge. *Nucleic Acids Res.* **47**, D506–D515 (2019).
35. A. Ikegami *et al*., The CHLI1 subunit of *Arabidopsis thaliana* magnesium chelatase is a target protein of the chloroplast thioredoxin. *J. Biol. Chem.* **282**, 19282–19291 (2007).
36. X. Liu *et al*., Structural insights into the N-terminal GIY-YIG endonuclease activity of *Arabidopsis* glutaredoxin AtGRXS16 in chloroplasts. *Proc. Natl. Acad. Sci. U.S.A.* **110**, 9565–9570 (2013).
37. K. Motohashi, F. Koyama, Y. Nakanishi, H. Ueoka-Nakanishi, T. Hisabori, Chloroplast cyclophilin is a target protein of thioredoxin. Thiol modulation of the peptidyl-prolyl *cis-trans* isomerase activity. *J. Biol. Chem.* **278**, 31848–31852 (2003).
38. P. G. Blommel *et al*., Crystal structure of gene locus At3g16990 from *Arabidopsis thaliana*. *Proteins* **57**, 221–222 (2004).
39. L. Men, Y. Wang, The oxidation of yeast alcohol dehydrogenase-1 by hydrogen peroxide *in vitro*. *J. Proteome Res.* **6**, 216–225 (2007).
40. S. Dumont *et al*., *Arabidopsis thaliana* alcohol dehydrogenase is differently affected by several redox modifications. *PLoS One* **13**, e0204530 (2018).
41. N. Colaert, K. Helsens, L. Martens, J. Vandekerckhove, K. Gevaert, Improved visualization of protein consensus sequences by iceLogo. *Nat. Methods* **6**, 786–787 (2009).
42. V. Gupta, K. S. Carroll, Sulfenic acid chemistry, detection and cellular lifetime. *Biochim. Biophys. Acta* **1840**, 847–875 (2014).
43. G. Roos, N. Foloppe, J. Messens, Understanding the pK_a of redox cysteines: The key role of hydrogen bonding. *Antioxid. Redox Signal.* **18**, 94–127 (2013).
44. D. A. Meekins, C. W. Vander Kooi, M. S. Gentry, Structural mechanisms of plant glucan phosphatases in starch metabolism. *FEBS J.* **283**, 2427–2447 (2016).
45. H. M. Lander *et al*., A molecular redox switch on $p21^{ras}$. Structural basis for the nitric oxide-$p21^{ras}$ interaction. *J. Biol. Chem.* **272**, 4323–4326 (1997).
46. J. Heo, S. L. Campbell, Mechanism of $p21^{Ras}$ S-nitrosylation and kinetics of nitric oxide-mediated guanine nucleotide exchange. *Biochemistry* **43**, 2314–2322 (2004).
47. S. E. Leonard, K. G. Reddie, K. S. Carroll, Mining the thiol proteome for sulfenic acid modifications reveals new targets for oxidation in cells. *ACS Chem. Biol.* **4**, 783–799 (2009).
48. M. Chatterjee, B. M. Paschal, Disruption of the Ran system by cysteine oxidation of the nucleotide exchange factor RCC1. *Mol. Cell. Biol.* **35**, 566–581 (2015).
49. J. M. Denu, K. G. Tanner, Specific and reversible inactivation of protein tyrosine phosphatases by hydrogen peroxide: Evidence for a sulfenic acid intermediate and implications for redox regulation. *Biochemistry* **37**, 5633–5642 (1998).
50. J.-S. Kim, T. Y. Huang, G. M. Bokoch, Reactive oxygen species regulate a slingshot-cofilin activation pathway. *Mol. Biol. Cell* **20**, 2650–2660 (2009).
51. Z. Jandova, Z. Trosanova, V. Weisova, C. Oostenbrink, J. Hritz, Free energy calculations on the stability of the 14-3-3ζ protein. *Biochim. Biophys. Acta.* **1866**, 442–450 (2018).
52. Y. Liu, C. He, A review of redox signaling and the control of MAP kinase pathway in plants. *Redox Biol.* **11**, 192–204 (2017).
53. R. Desikan, J. T. Hancock, K. Ichimura, K. Shinozaki, S. J. Neill, Harpin induces activation of the Arabidopsis mitogen-activated protein kinases AtMPK4 and AtMPK6. *Plant Physiol.* **126**, 1579–1587 (2001).
54. D. Ortiz-Masia, M. A. Perez-Amador, J. Carbonell, M. J. Marcote, Diverse stress signals activate the C1 subgroup MAP kinases of *Arabidopsis*. *FEBS Lett.* **581**, 1834–1840 (2007).
55. R. Dóczi *et al*., The *Arabidopsis* mitogen-activated protein kinase kinase MKK3 is upstream of group C mitogen-activated protein kinases and participates in pathogen signaling. *Plant Cell* **19**, 3266–3279 (2007).
56. H. Nakagami, H. Soukupová, A. Schikora, V. Žárský, H. Hirt, A mitogen-activated protein kinase kinase kinase mediates reactive oxygen species homeostasis in *Arabidopsis*. *J. Biol. Chem.* **281**, 38697–38704 (2006).
57. D. Dorin *et al*., An atypical mitogen-activated protein kinase (MAPK) homologue expressed in gametocytes of the human malaria parasite *Plasmodium falciparum*. Identification of a MAPK signature. *J. Biol. Chem.* **274**, 29912–29920 (1999).
58. B. Wang *et al*., Analysis of crystal structure of *Arabidopsis* MPK6 and generation of its mutants with higher activity. *Sci. Rep.* **6**, 25646 (2016).
59. Á. Garai *et al*., Specificity of linear motifs that bind to a common mitogen-activated protein kinase docking groove. *Sci. Signal.* **5**, ra74 (2012).
60. J. A. Smith *et al*., Creation of a stress-activated p90 ribosomal S6 kinase. The carboxyl-terminal tail of the MAPK-activated protein kinases dictates the signal transduction pathway in which they function. *J. Biol. Chem.* **275**, 31588–31593 (2000).
61. A. Reményi, M. C. Good, W. A. Lim, Docking interactions in protein kinase and phosphatase networks. *Curr. Opin. Struct. Biol.* **16**, 676–685 (2006).
62. T. Tanoue, M. Adachi, T. Moriguchi, E. Nishida, A conserved docking motif in MAP kinases common to substrates, activators and regulators. *Nat. Cell Biol.* **2**, 110–116 (2000).
63. J. D. Keyes *et al*., Endogenous, regulatory cysteine sulfenylation of ERK kinases in response to proliferative signals. *Free Radic. Biol. Med.* **112**, 534–543 (2017).
64. J. Wu *et al*., Autophosphorylation in vitro of recombinant 42-kilodalton mitogen-activated protein kinase on tyrosine. *Proc. Natl. Acad. Sci. U.S.A.* **88**, 9508–9512 (1991).
65. J. Van Leene *et al*., A tandem affinity purification-based technology platform to study the cell cycle interactome in *Arabidopsis thaliana*. *Mol. Cell. Proteomics* **6**, 1226–1238 (2007).
66. J. Yang, K. A. Tallman, N. A. Porter, D. C. Liebler, Quantitative chemoproteomics for site-specific analysis of protein alkylation by 4-hydroxy-2-nonenal in cells. *Anal. Chem.* **87**, 2535–2541 (2015).
67. Y. Perez-Riverol *et al*., The PRIDE database and related tools and resources in 2019: Improving support for quantification data. *Nucleic Acids Res.* **47**, D442–D450 (2019).
68. J. Huang *et al*., Self-protection of cytosolic malate dehydrogenase against oxidative stress in Arabidopsis. *J. Exp. Bot.* **69**, 3491–3505 (2018).